AD-A038 834 ROME AIR DEVELOPMENT CENTER GRIFFISS AFB N Y F/G 9/5
ANALYSIS OF A DUAL FREQUENCY ARRAY TECHNIQUE.(U)
JAN 77 R J MAILLOUX, H STEYSKAL
UNCLASSIFIED RADC-TR-77-48 NL

END

DATE FILMED
5-77

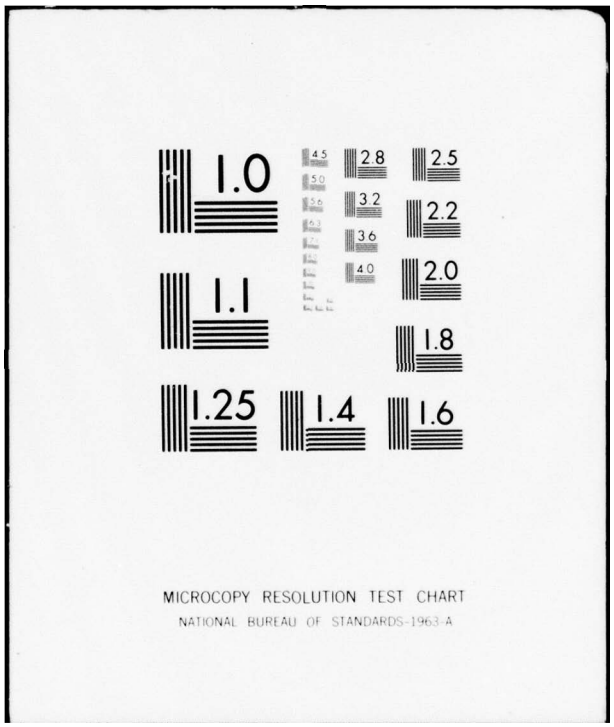
1.0
1.1
1.25
1.4
1.6
1.8
2.0
2.2
2.5
2.8
3.2
3.6
4.0
4.5
5.0
5.6
6.3
MICROCOPY RESOLUTION TEST CHART
NATIONAL BUREAU OF STANDARDS-1963-A

RADC-TR-77-48
IN-HOUSE REPORT
JANUARY 1977

Analysis of a Dual Frequency Array Technique

R.J. MAILLOUX
H. STEYSKAL

ROME AIR DEVELOPMENT CENTER
AIR FORCE SYSTEMS COMMAND
GRIFFISS AIR FORCE BASE, NEW YORK 13441

This report has been reviewed by the RADC Information Office (OI) and is releasable to the National Technical Service (NTIS). At NTIS it will be releasable to the general public, including foreign nations.

This technical report has been reviewed and approved for publication.

APPROVED:

PHILIPP BLACKSMITH
Branch Chief,
Antenna and Radar Techniques Branch

APPROVED:

WILLIAM B. GOGGINS, Lt Colonel, USAF
Acting Chief
Electromagnetic Sciences Division

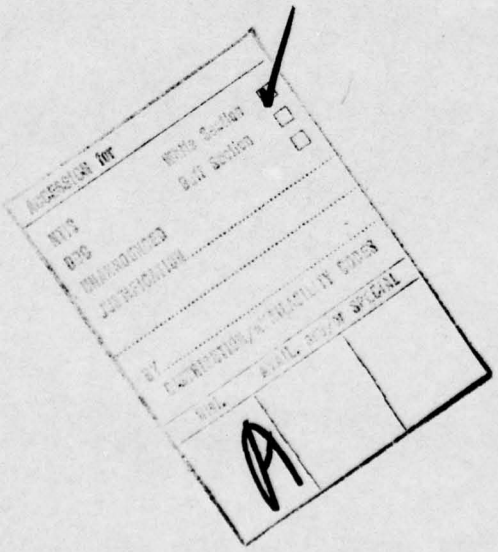

FOR THE COMMANDER: John P. Huss

Plans Office

Unclassified

SECURITY CLASSIFICATION OF THIS PAGE (When Data Entered)

REPORT DOCUMENTATION PAGE	READ INSTRUCTIONS BEFORE COMPLETING FORM
1. REPORT NUMBER: RADC-TR-77-48	2. GOVT ACCESSION NO. / 3. RECIPIENT'S CATALOG NUMBER
4. TITLE (and Subtitle): ANALYSIS OF A DUAL FREQUENCY ARRAY TECHNIQUE.	5. TYPE OF REPORT & PERIOD COVERED: Inhouse
	6. PERFORMING ORG. REPORT NUMBER
7. AUTHOR(s): R.J. Mailloux, H. Steyskal	8. CONTRACT OR GRANT NUMBER(s)
9. PERFORMING ORGANIZATION NAME AND ADDRESS: Deputy for Electronic Technology (RADC), Hanscom AFB, Massachusetts 01731	10. PROGRAM ELEMENT, PROJECT, TASK AREA & WORK UNIT NUMBERS: 62702F, ILIR5B01
11. CONTROLLING OFFICE NAME AND ADDRESS: Deputy for Electronic Technology (RADC), Hanscom AFB, Massachusetts 01731	12. REPORT DATE: January 1977
	13. NUMBER OF PAGES: 28
14. MONITORING AGENCY NAME & ADDRESS (if different from Controlling Office)	15. SECURITY CLASS. (of this report): Unclassified
	15a. DECLASSIFICATION/DOWNGRADING SCHEDULE

16. DISTRIBUTION STATEMENT (of this Report)

Approved for public release; distribution unlimited.

17. DISTRIBUTION STATEMENT (of the abstract entered in Block 20, if different from Report)

16 ILIR 17 5B

18. SUPPLEMENTARY NOTES

This effort was funded in part by the Laboratory Directors' Fund.

19. KEY WORDS (Continue on reverse side if necessary and identify by block number)

Antennas
Multifrequency
Wideband antenna

20. ABSTRACT (Continue on reverse side if necessary and identify by block number)

This report presents analytical results that describe the radiating properties of a new element for a dual frequency phased array. This basic element operates over two frequency bands which are separated by about an octave. The analysis considers the array element excited by two waveguides for high frequency operation, and includes an evaluation of the element radiation properties at both frequency bands. The analysis of radiation is carried out for the case of H-plane scan, which is expected to be the most severe test

DD FORM 1 JAN 73 1473 EDITION OF 1 NOV 65 IS OBSOLETE

Unclassified

SECURITY CLASSIFICATION OF THIS PAGE (When Data Entered)

309050

20. Abstract (Continued)

of the element's scanning behavior. Computed results indicate that the structure radiates efficiently within the two bands and operates free from anomalous behavior over substantial scan angles. These results demonstrate the feasibility and practicality of the basic concept.

Contents

Illustrations

Analysis of a Dual Frequency Array Technique

I. INTRODUCTION

The growing number of Air Force tactical and communication satellites place a continually increasing burden on aircraft antenna systems as presently conceived. The development of new array concepts to allow a single array to provide two independently scanned beams in separate frequency ranges, would aid in relieving the demand for aircraft station locations.

The possibility of combining two or more phased arrays in such a way as to fully share the same location, has intrigued researchers for several years. Some solutions to this problem are available and range from very wideband arrays[1-4] which can direct several beams on a time shared basis – but require an excessive

(Received for publication 26 January 1977)

1. Byron, E.V., and Frank, J. (1968) Lost beams from a dielectric covered phased-array aperture, IEEE Trans. G-AP AP-16(No. 4):496-499.

2. Byron, E.V., and Frank, J. (1968) On the correlation between wideband arrays and array simulators, IEEE Trans. G-AP AP-16(No. 5):601-603.

3. Laughlin, G.L., Byron, E.V., and Cheston, T.C. (1972) Very wideband phased-array antenna, IEEE Trans. G-AP AP-20(No. 6):699-704.

4. Chen, C.C., Wong, N.S., and Tang, R. (1973) Ultra Wideband Phased Arrays, Final Report, Contract F19628-72-C-0224, AFCRL-TR-73-0569.

number of control elements at the lower frequencies – to interlaced arrays[5-8] in which the total aperture is subdivided into ingeneous brickwork patterns of various size elements, with each frequency occupying a portion of the total aperture.

The concept investigated in this report was an outgrowth of a search for a new kind of dual-band array. It had to be subject to the constraints that each frequency band use the full aperture, that the array be excited by a separate corporate feed at each frequency (this to allow simultaneous, individually pointed beams), and that each corporate feed have the minimum number of phase shifters consistent with its scanning requirements. These constraints led to a rethinking of the dual-band problem, and to an array of the waveguide elements shown in Figure 1.

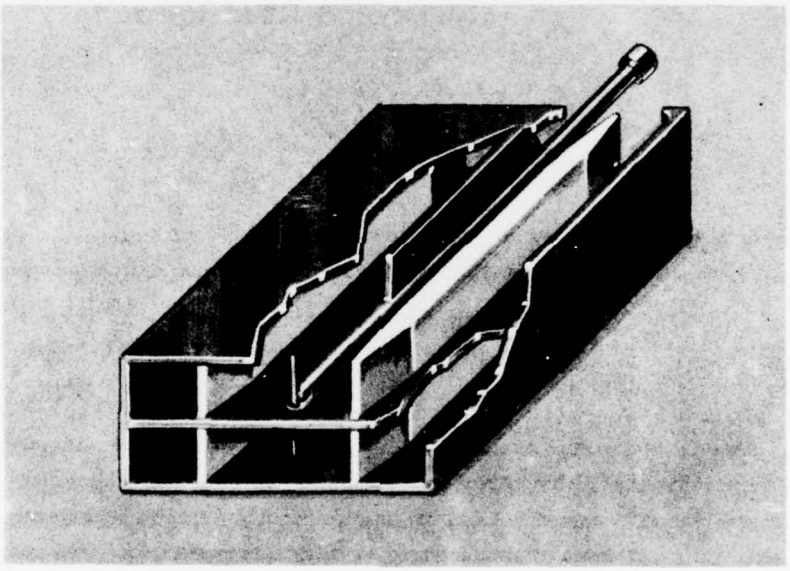

Figure 1. Basic Dual Frequency Array Element

5. Hsiao, J.K. (1971) Analysis of interleaved arrays of waveguide elements, IEEE Trans. G-AP AP-19(No. 7):729-735).

6. Boyns, J.F., and Provencher, J.H. (1972) Experimental results on a multi-frequency array antenna, IEEE Trans. G-AP AP-20(No. 1):106-107.

7. Hsiao, J.K. (1972) Computer aided impedance matching of an interleaved waveguide phased array, IEEE Trans. G-AP AP-20(No. 4):505-506.

8. Harper, W.H., Thrift, W.L., and Hailey, R.F. (1972) A Dual-Band Array Antenna, NRL Report No. 7369, Naval Research Laboratory.

The element shown in Figure 1 is made to operate at two independent frequencies by designing two circuits into the same microwave waveguide, and by dielectrically loading the waveguides so that the two signals do not interfere. With proper design the higher frequency signal can have the appropriate phase relationships across the final aperture to scan its beam over relatively wide angular sectors, and the lower frequency scans in the manner of a conventional phased array with a uniform phase across each element. The element consists of a waveguide bifurcated across the H-plane and loaded with four dielectric slabs as shown in Figure 1. The element size and thus the array interelement spacing is consistent with conventional practice for wide angle scanning at the lower frequency band. This low frequency circuit is excited by a probe as shown in Figure 1 or by a probe across a ridge loaded waveguide.

The high frequency circuit consists of four feed waveguides with tapered transitions into dielectrically loaded sections as shown in Figure 1. The waveguides are excited by conventional transitions from coaxial lines or by other waveguides with phase shifters; these details have been omitted in all figures. The purpose of the dielectric loading is to confine the fields very close to the dielectric slabs, and when this is done properly the central H-plane divider between two adjacent waveguides (the central wall divider indicated in Figure 1) can be removed without any substantial coupling of the adjacent waveguides. This wall is removed in the front part of the circuit and a probe for exciting the lower frequency signal is also mounted in the center of the oversize waveguide. This probe does not interfere with the high frequency signals traveling down the guide because they remain confined very closely to the dielectric slabs. Some tapering of the slabs is useful near the radiating aperture to improve scan match.

The crucial feature of this high frequency circuit is that the adjacent high frequency signals couple minimally – except at the radiating aperture – and so to first order the H-plane field distribution across the element aperture is the same as that incident from the feed waveguides. Thus, again to first order, the difference between feed waveguide phases for two adjacent launchers is the same as that required to form a beam at the given scan angle. An alternative perspective on the question of H-plane independence will be presented later by means of a discussion of the waveguide higher order modal propagation.

The low frequency circuit consists of two waveguides approximately twice the width of each of the high frequency waveguides and approximately the same height as the high frequency waveguides. These waveguides are excited in pairs by means of a dipole probe connected to a coaxial line. The height of each pair is approximately twice that of the high frequency guide. The dipole probe is placed a fixed distance "L" in front of where the high frequency waveguides join the double width waveguide, and the E-plane septum and high frequency waveguides serve as a

shorted back-plate for the low frequency probe. The low frequency waveguide itself will operate well below the cutoff of the particular waveguide type, because of its heavy dielectric loading.

In this manner, and depending upon design constraints, the array element operates within two distinct frequency bands. These frequencies should nominally differ by a factor of two for wide angle scanning at each frequency, and the usable bandwidth about each nominal frequency is a function of the required scan angle, impedance matching conditions, and element geometry.

Since an array of the dual model elements can be expected to exhibit the usual problems associated with scanned waveguide arrays, it is important at the outset to investigate this scanning in some detail.

This report treats the fundamental problem of H-plane scanning for the dual band, infinite array. The array periodicity in this plane is quite unconventional, and so one might expect that any major problems due to element spacings and the complexity of the periodic cell would be more important in this plane than in the E-plane. The elements are assumed to have zero thickness walls perpendicular to the E-plane and therefore the array fields are uniform in this plane, $(\partial/\partial_Y = 0)$.

2. MODES IN THE FEED WAVEGUIDES AND THE ARRAY ELEMENT WAVEGUIDE: DESIGN IMPLICATIONS

The behavior of waveguides partially filled with dielectric is well known to those who have designed ferrite isolators. This behavior is widely documented for high dielectric constant slabs placed across the center of the guide in the E-plane, and for such structures, one can choose slab thickness and dielectric constant to result in waveguide fields that are very intense within the dielectric but small elsewhere in the waveguide. It is also commonly known that, for these cases, removal of the waveguide E-plane walls barely perturbs the field. This fact allows the dual slab array element waveguide to be excited by two conventional dielectric slab-loaded waveguides as shown in Figure 1, and the assumption implied above is that the two exciting feed waveguides establish independent fields that are then used to control the field at the radiating aperture. For intuitive purposes, these fields are considered as unperturbed from the field distribution for the feed waveguide with a single slab. In fact, however, the dual slab array element waveguide cannot support this incident field exactly, and what is described in the introduction as "coupling" between these "independent" fields is primarily a consequence of the difference in propagation constants between the two lowest order modes in the dual slab guide. A brief description of these modes for single and double slab waveguides and their implications for design follows.

For the present case the electric field is independent of Y and has only one Y directed component. Therefore, scalar, transverse electric mode functions suffice to describe the fields, and for the waveguide of Figure 2 they are defined in the three specified regions by the following equations:

$$e_n = A_n e^{-j \arg P_n} \sin P_n \phi \qquad 0 \le \phi \le \alpha$$

$$e_n = D_n \sin (Q_n \phi + \eta_n) \qquad \alpha \le \phi \le \alpha + \delta \qquad (1)$$

$$e_n = \begin{cases} C_n \cos P_n (1 - \phi) & n \text{ odd} \\ C_n e^{-j \arg P_n} \sin P_n (1 - \phi) & n \text{ even} \end{cases} \qquad \alpha + \delta \le \phi \le 1$$

where

$$\phi = \frac{x + a/2}{a} \ ,$$

$$\alpha = \frac{C_1}{a/2} \quad \text{and}$$

$$\delta = \frac{t}{a/2} \ .$$

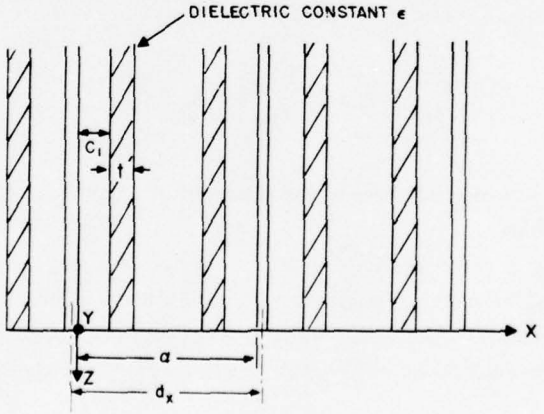

Figure 2. Section of Infinite Dual Frequency Array (H-Plane Scan)

This notation is chosen to correspond to that used by Seckelmann,[9] who also defines the relative amplitudes of A, C, D, P and Q for TE modes in this type of waveguide. The parameter η replaces the function θ as defined by Seckelmann. The parameter D is used to normalize the orthogonal[10] set $\{e_n\}$ so that

$$(e_m, e_n) = \int_{\phi=0}^{2} e_m \cdot e_n \, d\phi = \delta_{mn} \quad . \tag{2}$$

Subscripts "n" have been introduced above to distinguish the various modes.

Seckelmann shows waveguide field distributions and ranges of propagation constants for various waveguide and slab geometries, and gives an equation for the propagation constant. The modes for "n" even are antisymmetric about the center of the dual slab waveguide, and hence are also solutions for the single slab feed waveguides if the wall thickness between adjacent feed waveguides is zero.

Figure 3 shows the n = 1 and n = 2 field distributions for a dual slab waveguide with the following parameters:

$a = 4.755$ cm $= d_x$

$t = 0.635$ cm

$c_1 = 0.825$ cm

$\epsilon = 9$

Frequency = 6 GHz .

These symmetric and antisymmetric distributions are remarkably similar and their propagation constants are also nearly the same:

$$\beta_{10} = \frac{2\pi}{\lambda_{g_{10}}} \left(\frac{a}{2}\right) = 6.709 \quad ; \quad \beta_{20} = \frac{2\pi}{\lambda_{g_{20}}} \left(\frac{a}{2}\right) = 6.679$$

These constants are normalized to the waveguide half-width in keeping with the definitions by Seckelmann.

The near identity in propagation constant is a major design factor because it determines the degree to which signals can be considered to propagate independently along the two dielectric slabs. As indicated earlier, the n = 2 mode also satisfies the boundary conditions in the single slab waveguides, but the pure n = 2

---

9. Seckelmann, R. (1966) Propagation of TE modes in dielectric loaded waveguides, IEEE Trans. Microwave Theory and Techniques MTT-14:518-527.

10. Collin, R. E. (1951) Field Theory of Guided Waves, New York, McGraw Hill.

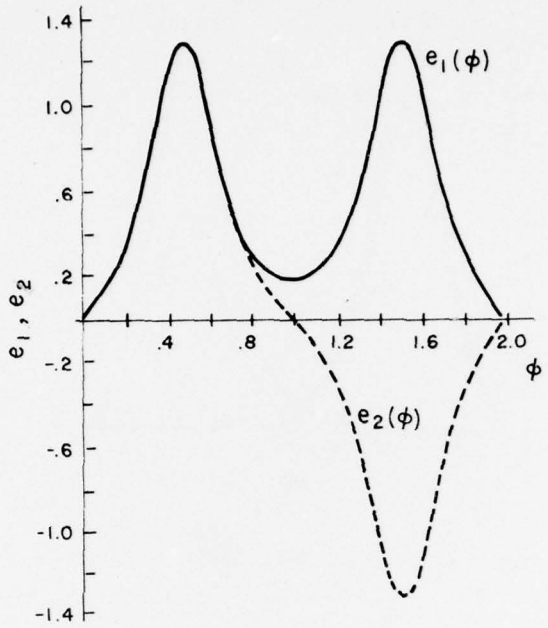

Figure 3. Modal Field Amplitudes e_1, e_2

mode is only excited in the dual slab waveguide when the two feed guides are phased 180° apart. The n = 1 mode does not satisfy the single slab waveguide boundary conditions, and so there is actually no mode in the dual slab waveguide that corresponds exactly to the independent excitation by only one of the feed guides. However, the similarity between symmetric and antisymmetric distributions and their wavenumbers assures that by superimposing these modes in the dual slab waveguide, one can approximately match this incident distribution at the input junction. Since the propagation constants are not identical the field distribution changes as a function of distance from the junction, and this factor must be accounted for in design. The example given above illustrates one choice of parameters that obviates the need for any special care, because the difference between normalized propagation constants is 0.030 and thus if the two modes start out in phase, the required distance for them to become separated by 180° is $\pi/0.030$ or approximately 105 half guide widths. Clearly this rate of dispersion is so slow as to be unimportant, but the use of lower dielectric constants or thinner dielectric slabs can create a substantial problem and must be considered when choosing dimensions.

Figure 4 shows three sets of data corresponding to the case of a junction between two single and one double slab waveguide, with only one of the single slab guides excited. These curves show the field at normalized distances of 0, 40, and

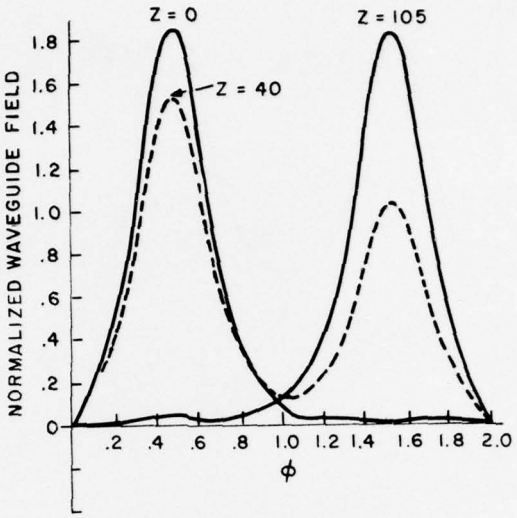

Figure 4. Normalized Waveguide Fields

105 waveguide half widths from the junction and so correspond approximately to inphase slightly less than 90 degrees and 180 degrees of phase difference between the modes. The analysis leading to Figure 4 will be sketched briefly in the next section, and accounts for all of the higher order modal effects present at the junction where the E-plane bifurcation ends. The curves serve to illustrate how the sum of propagating modes can become distorted because of the difference in relative propagation constants. Unfortunately, this effect cannot be eliminated by merely adjusting the relative phases at the single-slab waveguide feeds because these serve only to define the amplitude ratio of even to odd mode excitation, and not the phases of the two modes. Since full amplitude and phase control as required to counteract the dispersive effect would require use of a pair of hybrids, it is by far easier to choose the waveguide geometry and line lengths so that these adverse effects are minimized at center frequency.

Figure 5 shows several curves of normalized propagation constants β_{10} and β_{20} and β_{30} as a function of free space normalized wavenumber for three different dielectric slab configurations in the basic waveguide section with dimensions given earlier. These curves indicate that it is possible to choose operating bands at two different frequency ranges (one roughly double the other as required by scanning and lattice constraints). The low frequency range is characterized by propagation of only the 10 mode and the useful high frequency range by the near-identity of symmetric and antisymmetric model propagation constants. The useful upper limits to each of these ranges is the onset of the next higher order mode, the 20

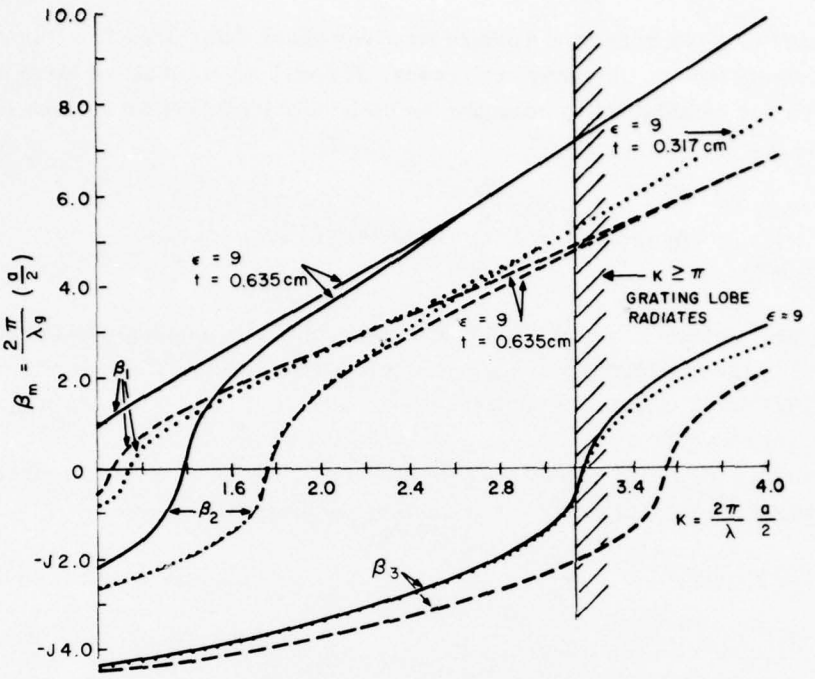

Figure 5. Propagation Constants for Fundamental Waveguides

mode for the low frequency range and the 30 mode for the high frequency range. Among the conclusions that can be drawn based upon these curves is that the use of the higher dielectric constant ($\epsilon = 9$) with 0.984 cm thick slabs results in the broadest usable high frequency range, but has its low frequency range limited by early onset of the propagating 20 mode. Using thinned slabs of the same material or reducing the dielectric constant of the material, raises the low frequency range at the expense of the high frequency bandwidth.

Other factors that influence waveguide and dielectric geometry selections include the degree of difficulty in designing coaxial transitions to the low frequency guide and the extent to which the low frequency probe assembly interacts with the high frequency fields. These tradeoffs cannot be made at this stage of development because they must be considered in the light of an array scanning in both planes, not merely one. However, early design results point to the relative difficulty of developing transitions to the heavily loaded waveguide with $\epsilon = 9$, and this must be traded off against the advantageous dispersion characteristic of that design.

A final design consideration is that it may be necessary to increase the relative dispersion between modes in order to optimize pattern control. An example

of this need is given in Section 3 where an added phase delay produces improved grating lobe response. In many such cases, Figure 5 shows that the extra phase dispersion can be obtained by reducing the dielectric thickness for a given length of guide.

3. EXCITATION OF THE HIGH FREQUENCY FIELDS AT THE BIFURCATED JUNCTION

The previous section described modal eigenfunctions for single and dual slab waveguides. This section presents an analysis of the junction between the single slab and dual slab waveguides subject to the condition $\partial/\partial_Y = 0$ and an infinitely thin bifurcation.

Figure 6 defines the geometry of the junction and both waveguides. Incident and reflected mode amplitudes are denoted by vectors

$$\bar{a}' = \{a'_n\} \quad \text{and} \quad \bar{r}' = \{r'_n\}$$

in the bifurcated waveguide region and

$$\bar{a} = \{a_n\} \quad \text{and} \quad \bar{r} = \{r_n\}$$

in the dual slab waveguide region. These model amplitudes are related by the scattering matrix that describes the junction and the section of dual slab waveguide between junction and aperture

$$\begin{pmatrix} \bar{r}' \\ \bar{r} \end{pmatrix} = \begin{pmatrix} S_{11} & S_{12} \\ S_{21} & S_{22} \end{pmatrix} \begin{pmatrix} \bar{a}' \\ \bar{a} \end{pmatrix} . \tag{3}$$

The amplitude coefficients a_n and r_n multiply the orthonormal electric modes e_n in the double slab waveguide, and the coefficients a'_n and r'_n multiply orthonormal electric modes f_n which are defined over the combined cross section of the two feedguides. S_{mn} denote matrices. The modes f_n of the feedguide pair, the modes e'_n of the single feedguide, and the modes e_n of the double slab guide are related in the following way. The e'-modes correspond to the antisymmetric e-modes and the only difference is a normalizing vector

$$e'_n = \begin{cases} \sqrt{2}\, e_{2n} \text{ over one feedguide} \\ 0 \quad \text{elsewhere} \end{cases} . \tag{4}$$

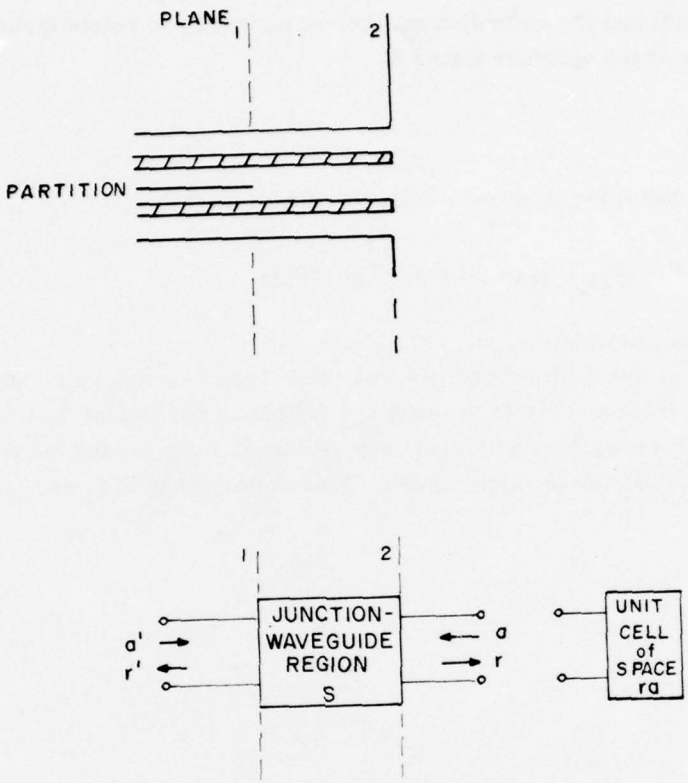

Figure 6. Definition of the Geometry of the Junction and both Waveguides. (a) Geometry of radiating waveguide, and (b) definition of waveguide reference planes

For the analysis, the modes f_n, which are symmetric and antisymmetric combinations of the e'-modes, are more convenient. They are

$$f_n = \begin{cases} \frac{1}{\sqrt{2}}\, e'\left(\frac{n+1}{2}\right) & \text{over lower guide} \qquad n = \text{odd}\ , \quad f_n \neq e'_n \\ \frac{1}{\sqrt{2}}\, e'\left(\frac{n+1}{2}\right) & \text{over upper guide} \qquad n = \text{even}\ , \quad f_n = e'_n \end{cases} \tag{5}$$

The modes f_n and e_n differ, when n = odd, because of the field zero at the bifurcation.

Using Eq. (3) and the reflection coefficient matrix Γ_a to relate incident and reflected waves at the aperture (plane 2)

$$\bar{a} = \Gamma_a \bar{r} \quad , \tag{6}$$

one obtains the following input reflection coefficient matrix:

$$\Gamma = (\bar{a}')^{-1} \bar{r}' = [S_{11} + S_{12} \Gamma_a (I - S_{22} \Gamma_a)^{-1} S_{21}] \tag{7}$$

where I is the identity matrix.

Evaluation of this matrix requires that each of the S-matrices be known. Then one can use the matrix above to evaluate the reflection coefficient in each of the input single slab waveguides with arbitrary excitation $A_1 e_1'$ for the lower guide (Figure 6a) and $A_2 e_1'$ for the upper guide. This corresponds to f_1 and f_2 with amplitudes:

$$\begin{aligned} a_1' &= \frac{1}{\sqrt{2}} (A_1 + A_2) \\ a_2' &= \frac{1}{\sqrt{2}} (A_1 - A_2) \\ a_n' &= 0 \qquad n \neq 1, 2 \quad . \end{aligned} \tag{8}$$

Likewise, the reflected dominant mode amplitudes R_1' and R_2' in each waveguide are given by:

$$\begin{aligned} R_1 &= \frac{1}{\sqrt{2}} (r_1' + r_2') \\ R_2 &= \frac{1}{\sqrt{2}} (r_1' - r_2') \end{aligned} \tag{9}$$

and using $\bar{r}' = \Gamma \frac{'}{\bar{a}}$ and the definition of Γ, one obtains for the reflected waves:

$$\begin{aligned} R_1 &= \frac{1}{2} [(\Gamma_{11} + \Gamma_{21})(A_1 + A_2) + (\Gamma_{12} + \Gamma_{22})(A_1 - A_2)] \\ R_2 &= \frac{1}{2} [(\Gamma_{11} - \Gamma_{21})(A_1 + A_2) + (\Gamma_{12} - \Gamma_{22})(A_1 - A_2)] \end{aligned} \tag{10}$$

where Γ_{mn} denote the mnth element of the matrix Γ.

These equations give the input reflection coefficients at the single slab waveguides for arbitrary excitation and include the multimodal reflection coefficient at the array aperture. There remains to solve the junction problem for the scattering matrix terms S_{mn}.

Defining E_1 and E_2 to be the transverse electric fields at planes 1 and 2, and H^i and X-directed incident magnetic field at plane 1, then E_1 may be obtained from the equation

$$2H^i = L'(E_1) + L(E_1) \tag{11}$$

where L' and L are the operators giving the H-field in terms of the E-field in a traveling wave in the regions to the left and right of plane 1, respectively. The H-plane is obtained by expanding E_1 in electric field modes and then multiplying each mode by its modal admittance (Y'_μ and Y_μ in the feedguide and dual slab guide, resp.) which gives

$$L'(E_1) = \sum_\mu (E_1, f_\mu)\, Y'_\mu f_\mu$$

$$L(E_1) = \sum_\mu (E_1, e_\mu)\, Y_\mu e_\mu \tag{12}$$

$$H^i = \sum_\mu a'_\mu Y'_\mu f_\mu \quad .$$

Here, the notation (E, e) is the conventional inner product. An approximate solution for (11) is found by Galerkin's method. Letting

$$E_1 \simeq \sum_{m=1}^{M} v_m f_m \tag{13}$$

and substituting (13) and (12) into (11) and taking the inner product of the resulting equation with the set $\{f_m\}^M$ reduces (11) to the following matrix equation for the unknown $\{v_m\}_1^{M'}$.

$$2Y\bar{a}' = C\bar{v}$$

where

$$Y' = \begin{pmatrix} Y'_1 & 0 \\ & \\ 0 & Y'_M \end{pmatrix} \quad ; \quad \bar{a}' = \begin{pmatrix} a'_1 \\ \vdots \\ a'_M \end{pmatrix} \quad ; \bar{v} = \begin{pmatrix} v_1 \\ \vdots \\ v_M \end{pmatrix} \tag{14}$$

$$C = (C_{mn}) = (C_{nm}) = \left(Y'_m \delta_{mn} + \sum_{\mu=1}^{N} Y_m B_{\mu m} B_{\mu n} \right)$$

$$B_{\mu m} = (e_\mu \ , \ f_m)$$

The S_{11} and S_{21} are given in terms of the above using

$$\bar{v} = \bar{a}' + \bar{r}' = 2C^{-1} Y' \bar{a}' \tag{15}$$

and therefore

$$S_{11} = \bar{r}'(\bar{a}')^{-1} = 2C^{-1} Y' - I \ . \tag{16}$$

The transmitted waves $\bar{r}$ in the dual band waveguide just inside of the array aperture, are obtained by equating the tangential E fields on both sides of the single slab/dual slab waveguide junctions and then transferring this field to the aperture.

Equating the tangential fields

$$E_1 = \sum_{n=1}^{M} v_n f_n = \sum_{m=1}^{M} r_m(0) \, e_m \tag{17}$$

which gives

$$r_m(0) = \sum_{n=1}^{M} v_n (f_n, e_m) \ .$$

At plane 2 and distance ℓ from the junction, the modes have been delayed $e^{-\gamma_n \ell}$ and therefore the waves incident upon the aperture are:

$$\overline{r} = S_{21}\overline{a}' = \overline{r}(\ell) = \phi\,\overline{r}(0) = \phi B \overline{v} = 2\phi B C^{-1} Y' \overline{a}' \tag{19}$$

where

$$\phi = (\phi_{mn}) = e^{-\gamma_n \ell}\,\delta_{mn}$$

and the B matrix with coefficients B_{mn} has been defined previously.

The remaining parameters which must be defined to solve Eq. (3) are the scattering matrices S_{12} and S_{22}. For this case, the field (a) is incident from the dual slab region. Following the same procedure for solving (11) as before, one obtains

$$2 B^{\dagger} Y \overline{a}(0) = C \overline{v} \tag{20}$$

where the diagonal matrix Y has coefficients $Y_{mn} = Y_m \delta_{mn}$. Since

$$\overline{a}(0) = \phi\,\overline{a} \tag{21}$$

and, this time

$$\overline{r}' = \overline{v} \tag{22}$$

it follows that

$$S_{12} = r'(a)^{-1} = 2 C^{-1} B^{\dagger} Y \phi \quad . \tag{23}$$

Similarly, S_{22} can be obtained as before by transferring the waves reflected from plane 1 to reference plane 2. This is done by first expressing E_1 in terms of $\{e_n\}$.

$$E_1 = \sum_m v_m f_m = \sum_m (a_m(0) + r_m(0))\, e_m \quad . \tag{24}$$

Again, taking the inner product with e_m gives

$$\bar{a}(0) + \bar{r}(0) = B\bar{v} \quad . \tag{25}$$

Substituting $\bar{a} = \phi \bar{a}^*(0)$ and $\bar{r} = \phi \bar{r}(0)$ gives

$$S_{22} = \bar{r}(\bar{a})^{-1} = \phi[2BC^{-1}B^{\dagger} Y - I]\phi \quad . \tag{26}$$

This completes the determination of the junction scattering matrix and hence the characterization of the network from the array face back to the single slab waveguides.

This analysis was used to compute the data presented in Figure 4, which shows the field distribution at various points along a dual slab waveguide that has been excited by the left waveguide of a two waveguide feed. Relevant dimensions are given on Figure 4. The dual slab is assumed to be infinitely long or properly terminated, so that the Γ_a matrix is null. This analysis has also been used to compute the fields for the same waveguide exciting a radiating element in an infinite array, the geometry of which is the subject of Section 4.

4. H-PLANE SCAN BEHAVIOR FOR AN INFINITE ARRAY

For the case of H-plane scanning with array elements having zero thickness walls perpendicular to the E-plane, the array is equivalent to a parallel plane structure shown in Figure 2. The electromagnetic field is thus derivable from a scalar potential function.

The solution proceeds by expanding the dual slab waveguide fields in terms of an infinite series of waveguide modes ($LSE_{p,0}$) and using these fields in the half space Greens function expansion.

The interior potential function for a mode with transverse incident field distribution $e_p(x)$ is:

$$\pi_p = e^{-\gamma_p Z} e_p(x) - \sum_{q=1}^{\infty} \Gamma_q e^{\gamma_q Z} e_q(x) \tag{27}$$

where γ_p and the γ_q are the modal propagation constants for the slab loaded waveguide.

The coefficients Γ_q give the amplitude and phase of the waves reflected from the aperture face ($Z = 0$) and include propagating and nonpropagating modes. The aperture field is:

$$E_{Y_p} = -j\omega \frac{\partial \pi_p}{\partial z} = j\omega \left[\gamma_p e_p(x) + \sum_{q=1}^{\infty} \Gamma_q \gamma_q e_q(x) \right] \quad . \tag{28}$$

Within the waveguides the magnetic field is given by

$$B_x = -\frac{\partial^2 \pi}{\partial z^2} \tag{29}$$

and in the exterior region it is obtained from the appropriate form of the half space Green's function. Assuming a periodic aperture field that forms a beam at the angle θ_o the aperture field in the M'th waveguide, is

$$E_Y = E_o e^{-jk_o u_o m d_x} \tag{30}$$

the exterior potential function for the infinite array, P'th incident mode, is written[11]

$$\pi(x, z) = \frac{-j}{\omega d_x} \int_{-a/2}^{a/2} dx' \, E_Y(x') \sum_{m=-\infty}^{\infty} e^{-j\beta_m (x-x')} \frac{e^{-\xi_m |z|}}{\xi_m} \tag{31}$$

and the magnetic field by:

$$B_{x_p} = -\frac{1}{d_x} \left[\gamma_p \int_{-a/2}^{a/2} e_p(x') \sum_{m=-\infty}^{\infty} e^{-j\beta_m (x-x')} \xi_m \, dx' \right.$$

$$\left. + \sum_{q=1}^{\infty} \Gamma_q \gamma_q \int_{-a/2}^{a/2} e_q(x') \sum_{m=-\infty}^{\infty} e^{-j\beta_m (x-x')} \xi_m \, dx' \right]$$

11. Mailloux, R.J. (1972) Surface waves anomalous wave radiation nulls on phased arrays of TEM waveguides with fences, IEEE Trans. AP-20(No. 2): 160-166.

where

$$\xi_m = \begin{cases} j\sqrt{k_o^2 - \beta_m^2} & \text{for} \quad \beta_m^2 > k_o^2 \\ \sqrt{\beta_m^2 - k_o^2} & \text{for} \quad \beta_m^2 < k_o^2 \end{cases}$$

$$\beta_m = k_o \left[u_o + \frac{m\lambda}{d_x} \right] \tag{32}$$

and

$$u_o = \sin \theta \quad .$$

Equating the interior and exterior magnetic field expressions at Z = 0, truncating the series at q = Q, multiplying by $e_\ell(x')$, using orthogonality and defining the integral

$$\text{Int}_q(\beta_m) = \int_{-a/2}^{a/2} e_q(x')\, e^{+j\beta_m x'}\, dx' \tag{33}$$

one obtains a set of Q equations for the Q coefficients of Γ_q for the incident p' the mode excitation:

$$\left[\delta_{p\ell}\, \gamma_p^2 - \frac{1}{d_x} \gamma_p \, \mathcal{J}_{p\ell} \right] = \sum_{q=1}^{Q} \Gamma_q \left[\gamma_q^2\, \delta_{q\ell} + \frac{1}{d_x} \gamma_q \, \mathcal{J}_{q\ell} \right] \tag{34}$$

for ℓ = 1 to Q and where

$$\mathcal{J}_{q\ell} = \sum_{m=-M}^{M} \xi_m \, \text{Int}_q(-\beta_m) \, \text{Int}_\ell(\beta_m) \quad . \tag{35}$$

Solution of the above matrix equation gives the waveguide field distribution at each aperture, and includes all of the mutual coupling effects for the infinite array. At the high frequency, two modes are incident and Eq. (34) must be solved twice and

the solutions combined appropriately for the combined two mode excitation. The truncation parameter M was varied between forty and several hundred in order to assure convergence.

As explained earlier, the combination of a symmetric and antisymmetric mode is required at the high frequency to produce an aperture distribution resembling the case wherein one dielectric slab is illuminated and the other not. Starting with that field configuration and neglecting the differences in the propagating constants of the TE_{10} and TE_{20} modes, one can represent an incident field that has approximately the same progressive phase distribution across the element as the corresponding phase between elements. This is done for the incident magnetic hertzian potential functions

$$\pi_p = e^{-\gamma_p z} e_p(x) \tag{36}$$

and with the total incident potential function for two modes (p = 1 and p = 2) so that

$$\pi = \pi_1 + R\pi_2 \quad . \tag{37}$$

The incident modal voltages are, therefore, multiplied by R and by the γ_p terms, and the ratio of the powers in the two incident modes is

$$P_{in_2} = |R|^2 (|\gamma_2|^3 / |\gamma_1|^3) \cdot P_{in_1} \quad . \tag{38}$$

Given this general definition of R, one can choose its value such that there is a zero in the two mode element pattern at the grating lobe position. In order to include the mutual coupling this must be done after the boundary value problems are solved for symmetric and antisymmetric incident modes, but for the purpose of this writeup it is convenient to choose an approximate value of R. If $\gamma_1 \sim \gamma_2$, one can assume a progressive phase input, resolve it into even and odd terms, and identify R with the odd mode amplitude coefficient. The result is

$$R_o \doteq j \tan\left(\frac{\pi d_x}{2\lambda} \sin\theta\right) \tag{39}$$

where θ is defined by the progressive phase shift between two apertures, which is $2\pi(dx/\lambda) \sin\theta$.

Figures 7 and 8 show the computed scan characteristics for an infinite array with C_1 = 0.8255 cm, t = 0.635 cm (solid) and C_1 = 1.143 cm, t = 0.3175 cm (dotted).

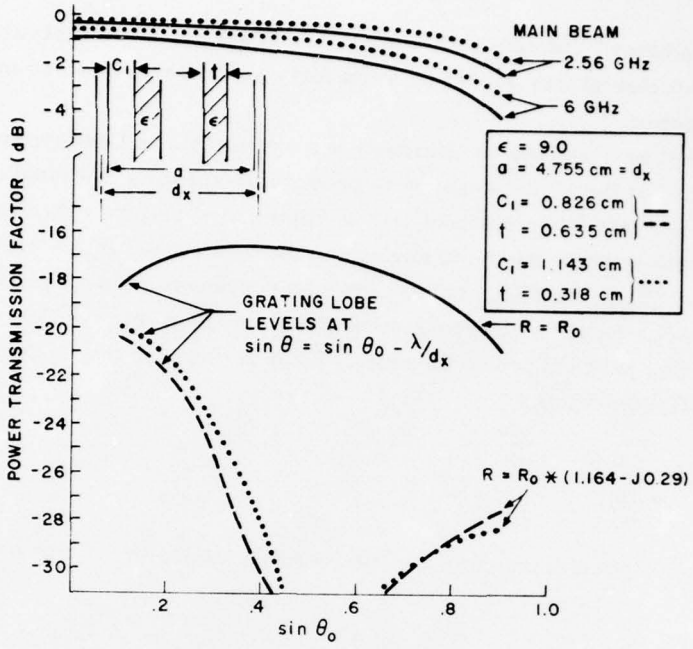

Figure 7. Scan Parameters of Dual Band Array (ϵ = 9)

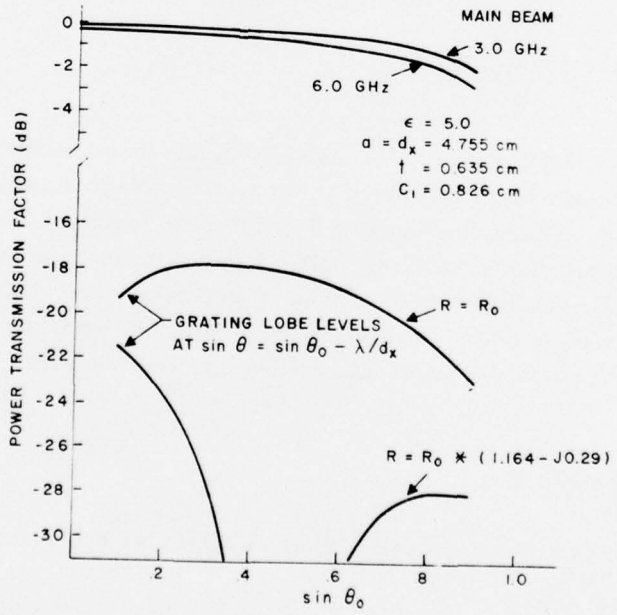

Figure 8. Scan Parameters of Dual Band Array (ϵ = 5)

The low frequency data of Figure 7 is computed at 2.5 GHz which is just below the onset of the LSE_{20} mode. The high frequency data (at 6 GHz) shows the height of the grating lobe at $\sin \theta = \sin \theta_o - \lambda/d_x$ as well as the main beam contribution at θ_o.

Choosing R_o as defined in Eq. (39) yields grating lobe levels below -16 dB with respect to the perfect transmission case. The dashed curve shows the grating lobe level obtained by choosing R empirically to be

$$R = R_o * (1.16 - j0.29) \quad . \tag{40}$$

This choice of R does not change the gain measurably, but for all but the relatively small scan angles it provides much better grating lobe suppression. This result shows that good suppression can be obtained with a value of R that has constant phase, so the relative phase of the odd and even modes is approximately a constant and independent of scan. The phase constant is not 90^o however, and so it is necessary to adjust the line length while using and perhaps necessarily increasing the relative difference in modal propagation constants given a section of the line in order to obtain the desired phase difference.

The dotted curves of Figure 7 show the results for a slab of $\epsilon = 9$ material with $\delta = 0.3175$ cm. Improved gain characteristics for this geometry support the conclusion that tapering would be an aid in scan-matching at the high frequency.

Figure 8 shows some of the corresponding data for the same waveguide geometry loaded with $\epsilon = 5$ dielectric. This choice does provide superior scan matching characteristics at the high frequency, but this advantage is achieved at the cost of somewhat greater differences in propagation constant between the TE_{20} and TE_{10} modes than for the $\epsilon = 9$ dielectric. The relative propagation constant difference is 0.030 for the $\epsilon = 9$ case, and is

$$(\beta_1 - \beta_2)\frac{a}{2} = 4.624 - 4.434 = 0.190$$

for the $\epsilon = 5$ case, and so the phase error buildup between even and odd modes is 0.19 radians for each half width of guide length. This could be a problem, depending upon the length of the dual mode section and is thus a factor to be considered in the design.

In all, these data give good assurance that the array structures of Figure 1 can provide good radiation characteristics over reasonable scan angles. The data show no blindness or other serious deficiencies resulting from cumulative mutual coupling. No attempt at scan matching has been made and the elements have not been matched at broadside; so there is room for substantial improvement in pattern control through the application of proper engineering techniques.

Figure 9 shows the magnitude and phase of the reflection coefficient at each of the two input waveguide ports for several values of the distance between the end of the E-plane bifurcation and the waveguide radiating aperture. These results include the two propagating modes only; all higher order modes have been assumed too strongly attenuated to be of consequence. The principle conclusion drawn from these results is that the reflection coefficients at each input port differ, thus making it difficult to design one matching unit in each waveguide that can provide true scan correction. Clearly, such correction can be achieved in the sense of an average tuning for the two waveguide element, but the problem is more difficult than for the conventional waveguide case. The second conclusion evident from the Figure 9 is that the introduction of the junction does not cause any noticable resonant behavior or pattern null within the scan sector. This conclusion assures at least for pure H-plane scan that the high frequency element can be excited by conventional waveguides without the risk of element blindness.

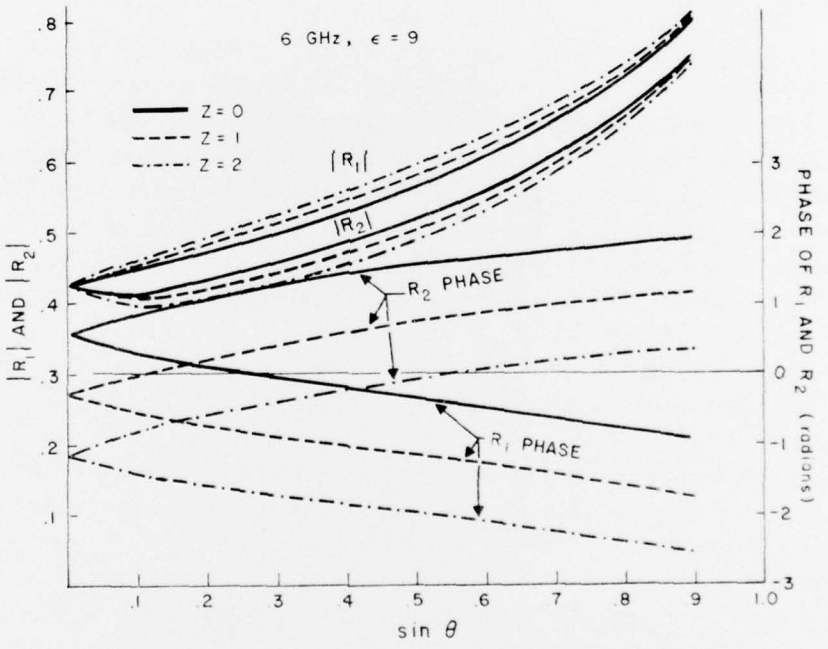

Figure 9. Feed Waveguide Reflection Coefficients for Scanned Array

5. CONCLUSION

This report has analyzed the behavior of a new dual frequency phased array element for the case of H-plane scan. The basic element uses dielectric loading to provide an efficient transmission path for the high frequency signal, which radiates through the same aperture as the lower frequency. This assures that the array can have good aperture efficiency at both frequencies.

The analysis includes a consideration of scattering at the junction between the single slab feed waveguides and the dual slab radiating waveguide. This junction analysis is used in conjunction with an analytical solution for the reflection coefficient of the radiating waveguide to provide a complete description of the reflection properties of the entire waveguide combination at the high frequency. Since the low frequency is excited by a dipole and uses the E-plane bifurcation to simulate a short circuited transmission line, the behavior at this frequency is independent of the feed waveguides. Scanning characteristics are recorded at both frequencies and indicate that the geometry exhibits no undesirable scan characteristics (blindness) at either frequency for reasonable scan angles in the H-plane. These data provide sufficient evidence to demonstrate the practicality of the basic element. Furthermore, they indicate that with sufficient concern for element design, this geometry can provide good aperture efficiency at broadside for both frequencies with potentially excellent scanning characteristics.

References

1. Byron, E. V., and Frank, J. (1968) Lost beams from a dielectric covered phased-array aperture, IEEE Trans. G-AP AP-16(No. 4):496-499.
2. Byron, E. V., and Frank, J. (1968) On the correlation between wideband *arrays and array simulators*, IEEE Trans. G-AP AP-16(No. 5):601-603.
3. Laughlin, G. L., Byron, E. V., and Cheston, T. C. (1972) Very wideband phased-array antenna, IEEE Trans. G-AP AP-20(No. 6):699-704.
4. Chen, C. C., Wong, N. S., and Tang, R. (1973) Ultra Wideband Phased Arrays, Final Report, Contract F19628-72-C-0224, AFCRL-TR-73-0569.
5. Hsiao, J. K. (1971) Analysis of interleaved arrays of waveguide elements, IEEE Trans. G-AP AP-19(No. 7):729-735.
6. Boyns, J. F., and Provencher, J. H. (1972) Experimental results on a multi-frequency array antenna, IEEE Trans. G-AP AP-20(No. 1):106-107.
7. Hsiao, J. K. (1972) Computer aided impedance matching of an interleaved waveguide phased array, IEEE Trans. G-AP AP-20(No. 4):505-506.
8. Harper, W. H., Thrift, W. L., and Hailey, R. F. (1972) A Dual-Band Array Antenna, NRL Report No. 7369, Naval Research Laboratory.
9. Seckelmann, R. (1966) *Propagation of TE modes in dielectric loaded waveguides*, IEEE Trans. Microwave Theory and Techniques MTT-14:518-527.
10. Collin, R. E. (1951) Field Theory of Guided Waves, New York, McGraw Hill.
11. Mailloux, R. J. (1972) Surface waves-anomalous wave radiation nulls on phased arrays of TEM waveguides with fences, IEEE Trans. AP-20(No. 2): 160-166.

MISSION
of
Rome Air Development Center

RADC plans and conducts research, exploratory and advanced development programs in command, control, and communications (C^3) activities, and in the C^3 areas of information sciences and intelligence. The principal technical mission areas are communications, electromagnetic guidance and control, surveillance of ground and aerospace objects, intelligence data collection and handling, information system technology, ionospheric propagation, solid state sciences, microwave physics and electronic reliability, maintainability and compatibility.

Printed by
United States Air Force
Hanscom AFB, Mass. 01731